Accepted Manuscript

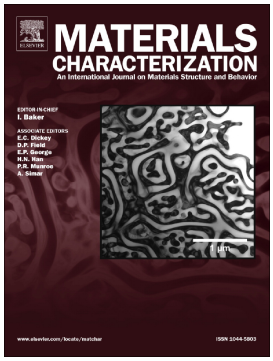

Formation of nanocrystalline structure in pearlitic steels by dry sliding wear

Rui Pan, Ruiming Ren, Chunhuan Chen, Xiujuan Zhao

PII: S1044-5803(17)30808-2
DOI: doi: 10.1016/j.matchar.2017.05.031
Reference: MTL 8692

To appear in: *Materials Characterization*

Received date: 19 March 2017
Revised date: 24 May 2017
Accepted date: 25 May 2017

Please cite this article as: Rui Pan, Ruiming Ren, Chunhuan Chen, Xiujuan Zhao , Formation of nanocrystalline structure in pearlitic steels by dry sliding wear, *Materials Characterization* (2017), doi: 10.1016/j.matchar.2017.05.031

This is a PDF file of an unedited manuscript that has been accepted for publication. As a service to our customers we are providing this early version of the manuscript. The manuscript will undergo copyediting, typesetting, and review of the resulting proof before it is published in its final form. Please note that during the production process errors may be discovered which could affect the content, and all legal disclaimers that apply to the journal pertain.

ACCEPTED MANUSCRIPT

Elsevier Editorial System(tm) for MATERIALS CHARACTERIZATION

Manuscript Draft
Manuscript Number:
Title: Formation of Nanocrystalline Structure in Pearlitic Steels by Dry Sliding Wear
Article Type: Regular Article
Keywords: nanocrystalline structure; pearlitic wheel steel; formation mechanism; sliding wear
Corresponding Author: Mrs. Xiujuan Zhao, Dr.
Corresponding Author's Institution: Dalian Jiaotong Unversity
First Author: Rui Pan
Order of Authors: Rui Pan; Ruiming Ren; Chunhuan Chen; Xiujuan Zhao

Abstract: Nanocrystalline grains, whose average size was approximately 35±5nm, were generated in the outermost layer of a pearlitic wheel steel by dry sliding wear. To explore the evolution of nanocrytalline grains, successive observations from the outermost layer of sliding wear to the undeformed matrix were done by scanning electron microscopy(SEM) and transmission electron microscopy (TEM). The investigations showed that the evolution process of nanometer-sized grains in pearlitic wheel steels included four steps: initially, pearlitic plastic deformation took place, lamellar spacing diminished, great amounts of dislocations occurred in ferrite, the thickness of ferrite lamellae decreased and some of ferrite lamellae fractured and dissolved; with increasing strains, considerable cementite started to dissolve into grains, and inside ferrite dislocations accumulated, tangled and formed dislocation walls, which cut ferrite into many short-rod shaped—and even equiaxed shaped dislocation cells; as strains continued to increase, dislocation cells gradually transformed into low-angle sub-boundaries. Accumulation and annihilation of dislocations and rotation of grains induced low-angle boundaries（LABs）to turn into high-angle boundaries(HABs), with the grains having random orientation. At this moment, cementite dissolution was relatively saturated and undissolved cementite particles scattered around the refined ferrite boundaries. Under higher strains and strain rates, refined ferrite grains repeatedly underwent plastic deformation, the formation of dislocation cells and the transformation from LABs to HABs, until finally the size of ferrite grains reached the stable minimum value and the refinement of grains ceased. Meanwhile, cementite continued to dissolve slightly due to dislocation accumulation. When dislocation accumulation rate and annihilation rate reached balanced, the dissolution of cementite ceased.

Key words: nanocrystalline structure; pearlitic wheel steel; formation mechanism; sliding wear

ACCEPTED MANUSCRIPT

Formation of Nanocrystalline Structure in Pearlitic Steels by Dry Sliding Wear

Abstract

Nanocrystalline grains, whose average size was approximately 35±5nm, were generated in the outermost layer of a pearlitic wheel steel by dry sliding wear. To explore the evolution of nanocrytalline grains, successive observations from the outermost layer of sliding wear to the undeformed matrix were done by scanning electron microscopy(SEM) and transmission electron microscopy (TEM). The investigations showed that the evolution process of nanometer-sized grains in pearlitic wheel steels included four steps: initially, pearlitic plastic deformation took place, lamellar spacing diminished, great amounts of dislocations occurred in ferrite, the thickness of ferrite lamellae decreased and some of ferrite lamellae fractured and dissolved; with increasing strains, considerable cementite started to dissolve into grains, and inside ferrite dislocations accumulated, tangled and formed dislocation walls, which cut ferrite into many short-rod shaped—and even equiaxed shaped dislocation cells; as strains continued to increase, dislocation cells gradually transformed into low-angle sub-boundaries. Accumulation and annihilation of dislocations and rotation of grains induced low-angle boundaries（LABs）to turn into high-angle boundaries(HABs), with the grains having random orientation. At this moment, cementite dissolution was relatively saturated and undissolved cementite particles scattered around the refined ferrite boundaries. Under higher strains and strain rates, refined ferrite grains repeatedly underwent plastic deformation, the formation of dislocation cells and the transformation from LABs to HABs, until finally the size of ferrite grains reached the stable minimum value and the refinement of grains ceased. Meanwhile, cementite continued to dissolve slightly due to dislocation accumulation. When dislocation accumulation rate and annihilation rate reached balanced, the dissolution of cementite ceased.

Key words: nanocrystalline structure; pearlitic wheel steel; formation mechanism; sliding wear

1. Introduction

Compared with metals and alloys which have coarse-grained structures, the ones with nanocrystalline structures often possess such numerous different properties as high strength,

ACCEPTED MANUSCRIPT

high hardness[1] and excellent tribological property[2]. This is because nanocrystalline structure owns two obvious characteristics: nanometer-sized grains and abundant boundaries[3,4]. Therefore, it is quite necessary to delve into the formation mechanism of nanocrystalline structure, which not only will help develop new materials for engineering applications, but also will upgrade the production of conventional materials. Previous experimental results showcase that different materials possess different grain refinement mechanisms, such as base-centered cubic (bcc) Fe[5], face-centered cubic (fcc) Cu[6], hexagonal close packed (hcp) pure Co[7], Ti [8] and Mg[9], which are single-phase materials. However, for pearlitic steels commonly used in engineering, their plastic deformation, for several decades, has been the subject of extensive investigations (the review paper of Langford[10]), but no one has delved into the formation mechanism of their nanocrystalline grains. Pearlite, a two-phase material, consists of softer ferrite matrixes and hard and brittle cementite plates. Although the formation mechanism of pure ferrite nanocrystalline grains is already known, when cementite exists in ferrite, the formation mechanism of nanocrystalline grains is, to some extent, different from that occurring in pure metals. Therefore, when delving into the formation of

ACCEPTED MANUSCRIPT

ACCEPTED MANUSCRIPT

pearlite nanocrystalline grains, it should be noted that changes of cementite and impacts of cementite on the ferrite transformation. In the process of plastic deformation, although cementite has limited ductility, cementite plates and ferrite in pearlite deform simultaneously[11-13]. Great amounts of research on cementite deformation capability has been done and it has been substantiated that inside pearlite, cementite plates indeed undergo severe deformation and slip and fracture planes of cementite are verified [14-19]. The cementite is a significantly stable metastable phase at room temperature[20]. Nevertheless, atom probe field ion microscopy (APFIM)[21-23], three dimensional atom probe (3DAP)[24,25] tests and internal friction[26], and Mossbauer[27,28] experiments indicated that masses of the cementite dissolve during deformation at room temperature. Through high resolution electron microscopy study, Languillaume indicated that when cementite fracture into the nanoscale particles, the surface energy will increase; in order to reduce the surface energy, fragmented cementite would eventually dissolve into ferrite[29]. However, this is inconsistent with the fact that the solubility of carbon in ferrite is limited and extremely low. However, it could be observed that when the pearlitic steel wires with tensile strength of 3930 MPa reached the maximum strain 4.2, cementite obviously fragmented into nanoscale particles, and part of cementite dissolved [30,31]. Consequently, during heavy plastic deformation of pearlite, cementite deformation and dissolution will be the focus of research. Inside the severely deformed pearlite, the size of cementite will reach nano-level category. In order to study this question, new techniques are needed to identify cementite.

Conventionally prepared scanning samples undergoes the corrosion of nutric acid and alcohol, but for nano-level grains, it often occurs that intracrystallines and boundaries are corroded together, which makes it harder to clearly identify the shape of grains. This article adopts special corrosion technique, which only corrodes the boundary of nano-level grains, and the shape of grains can be clearly observed under SEM.

Two research aims are included in this article: one is to discuss a mechanism of nanocrystalline structure formation for pearlitic wheel steels in the process of dry sliding wear based on SEM with special corrosion technology and TEM studies; the other is to consider the deformation and decomposition behavior of cementite.

2. Experimental methods

2.1 Samples Preparation

The material utilized in the experiment was a piece of CL65 pearlitic wheel steel with a chemical composition of 0.60-0.65 wt.% C, 0.80-0.95 wt.% Si, 0.78-0.85 wt.% Mn, 0.006-0.020 wt.% S, and 0.025 wt.% P(max). The hardness of sliding wear surface approximated 285HV. Fig.1(a) was the OM microstructure morphology of typical CL65 pearlitic wheel steel.

Sliding wear tests of the CL65 pearlitic steel were performed on MRH-5A ring-block tribometer. The block-on-ring contact configuration was depicted in Fig.1(b). The ring was made of U75V pearlitic rail steel with a hardness of 311HV. The test was done under dry condition at room temperature(25℃) of normal load of 150N, with ring rotation speed of 600rpm, wind cooling and a period of time about 30min for the dry sliding wear.

ACCEPTED MANUSCRIPT

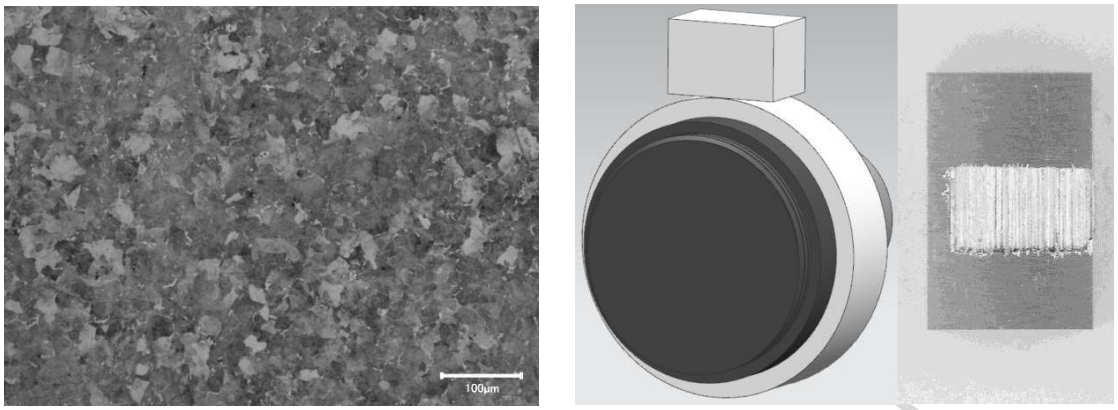

Fig.1(a) OM Microstructure Morphology Image of the CL65 Pearlitic Wheel Steel; (b) Illustration of the Wheel/Rail Specimens for Block-on-ring Sliding Wear.

2.2 Microstructure characterization

After dry sliding wear, the section microstructure of the specimen was observed by optical microscope (OM). The section hardness was measured by a FM-700 Vickers microhardness testing machine, with a load of 10gf and a loading time of 15s, in order that hardness variations with depths from the outermost layer could be studied. In order to investigate the grain refinement process and mechanism during sliding wear, it was necessary to examine the microstructure changes at different plastic deformation steps. The key to investigating the formation process and formation mechanism of nanocrystalline grains during dry sliding wear was determining microstructual transformations at different plastic deformation stages. Under the circumstances of forces, plastic deformation originated from the outermost layer and extended to the substrate along the direction vertical to the outermost layer, so deformation strains and strain rates decreased with increasing depths from the perspective of the section. In conclusion, the observation and investigation of the section microstructure at different depths could characterize the formation of nanocrystalline grains. The sectional samples for OM observations were corroded by standard metallographic procedures, while for SUPRA 55 field-emission SEM observations they were prepared by special corrosion technology, more details about the processing are in [32]. The sectional morphologies were observed on a SUPRA 55 field-emission SEM using secondary electron imaging mode. Transmission electron microscopy (TEM) specimens were sliced from sectional with different directions and prepared by a new method. The method for producing sectional TEM specimen with high residual stress on the outermost layer was described in [33]. Here was the process of TEM specimen preparation: 1mm slice, cut off from the sectional whose top surface was protected by silicon slice, was mechanically grinded to 3μm. The thin foil was adhered to a molybdenum ring by high-strength heat curing resin. Then a one-way mode was directly used for reducing the thickness to be smallest by ion. The method could obtain a sectional sample, for which the thinner area was suitable for observing by TEM from the surface to the inside. Detailed microstructural features of the sectional with different directions after sliding wear were observed by JEM 2100F field-emission TEM at 200KV and were analyzed by selected-area electron diffraction (SAED), conventional bright-field (BF), dark-field (DF) ,and high-resolution TEM (HRTEM) imaging.

ACCEPTED MANUSCRIPT

3. Results and Discussion

3.1 Optical Metallography and Microhardness

Fig. 2 showed the sectional microstructural micrographs after wear by OM. Specifically, Fig.2a and Fig. 2b showed the sections parallel and perpendicular to the direction of sliding wear respectively. After sliding wear, in the region adjacent to the surface of sliding wear, a fine-grained layer, bright and featureless, where grain morphology was hardly identified by OM, could be observed. The thickness of the fine-grained layer could be identified to be about 20μm. Beneath the fine-grained layer, a region with the plastic flow lines, clearly observed in Fig.2a, gradually bent towards the sliding direction, while such a feature was not obvious in Fig.2b. For the sectional micrograph, perpendicular to the direction of sliding wear, beneath the fine-grained layer, what could be identified was a well-compacted and defined layer, but material flow lines or grain boundaries could not be observed under OM. In short, beneath the fine-grained layer, the microstructure was pearlitite having undergone severe plastic deformation in Fig.2a, while such a feature was slightly different in Fig.2b, which needed further observation analysis by SEM.

Fig.3 exhibited variations of Vickers microhardness within the depth range from the sliding wear surface to undeformed pearlite substrate. From hardness curves, after dry sliding wear, the hardening layer of CL65 pearlitic wheel steel amounted to 50μm. The highest microhardness appeared on the outermost layer, reaching 715$HV_{0.01}$—close to that of the WEL caused by rolling-sliding contact friction in pearlitic rail steel (686HV)[34]. In addition, it could also be seen that the microhardness of the fine-grained layer on the outermost layer was more than twice that of the undeformed substrate. And in the hardening region, the Vickers microhardness distribution decreased gradually from the surface to the depth of 50μm. The measurement of the Vickers microhardness showed that the hardening layer was a typical gradient structure. In the following section, the gradient microstructure would be discussed in detail.

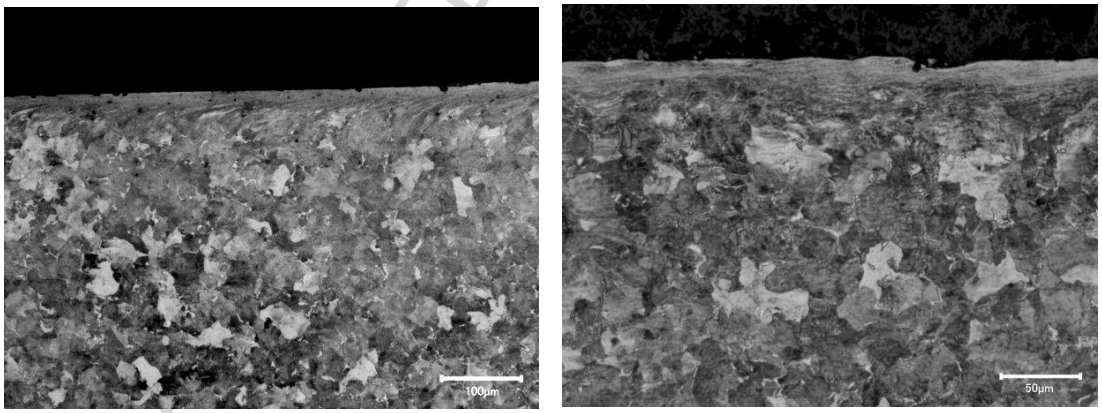

Fig. 2 The Sectional Microstructural Micrographs after wear by OM. (a) and (b) The sections Parallel and Perpendicular to the Direction of Sliding Wear Respectively

ACCEPTED MANUSCRIPT

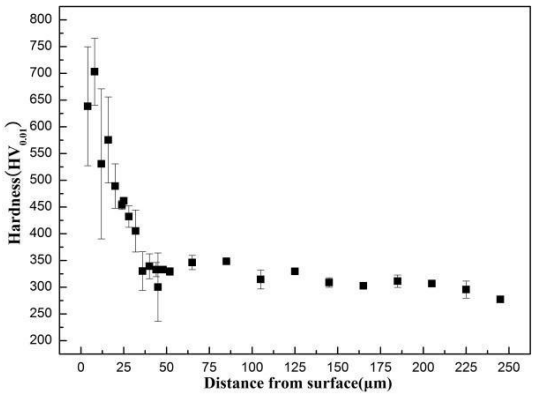

Fig.3 Vickers Microhardness Distribution Curves within the Depth Range from the Outermost Layer to the Substrate

3.2 Cross-sectional SEM morphologies

The overview of hardening region microstructure micrograph was shown in Fig. 4. Specifically, it exhibited the evolution of the microstructure at different plastic strains as the depth changes from the outermost layer to the inner undeformed substrate, with the depth range of approximately 50μm. A depth-dependent gradient microstructure was observed: a nanocrystalline region in the topmost surface of 1.5μm thick with characteristic size below 100nm, a submicrometer region in a depth span of 1.5 to 20μm, and a deformed region at 20~50μm deep. Deeper than 50μm was deformation-free substrate. Fig.4(b-e) was the further magnified images, thoroughly exhibiting the microstructure micrographs of fine-grained region at different depths. For comparison with the microstructure of the fine-grained region, the microstructure within a deformation-free region more than 1mm far from the outermost layer was observed, as was shown in Fig. 4(f). In this region, what could be spotted was pearlite lamellar structure, whose average lamellar spacing was 250-300nm, all straight without any inclination of deformation.

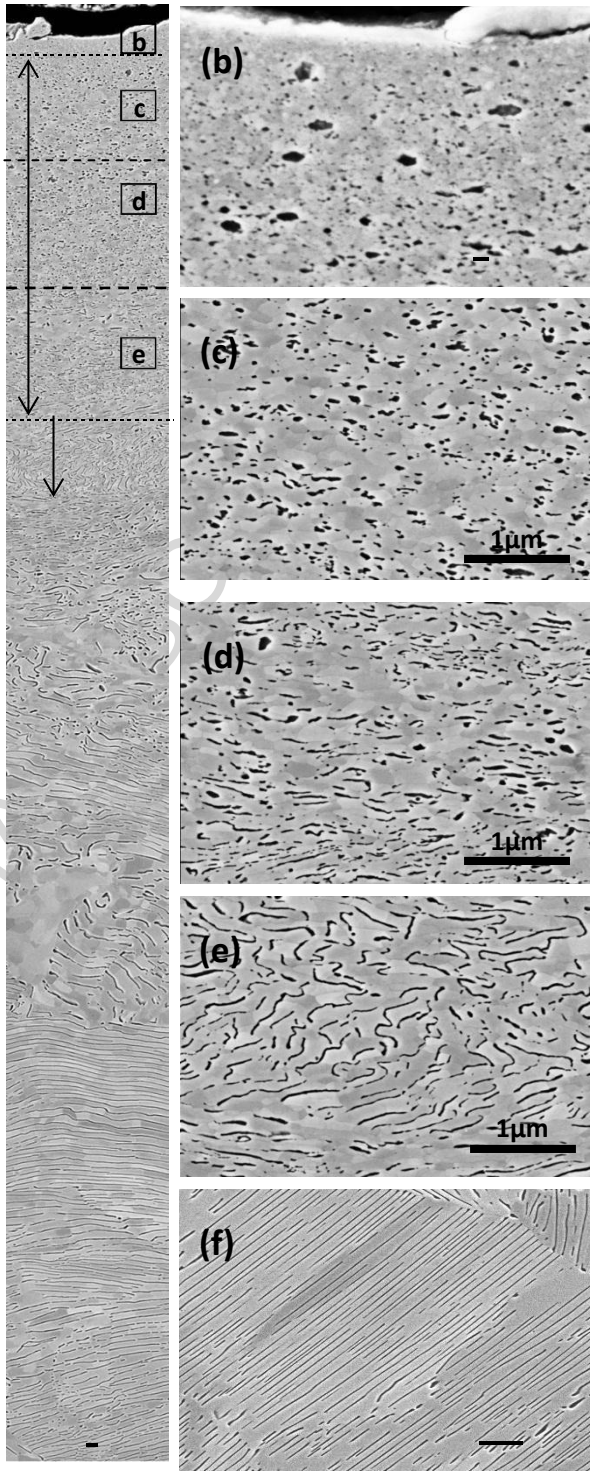

Fig.4(a) An Overview of Cross-sectional SEM Images of the Wheel Steel; (b-e) Three Typical Microstructures at Different Depths; (f) Undeformed Pearlite Microstructure from the

What was found in Fig. 4(a) was intense deformation at the depth span of 20 to 50μm below the fine-grained layer. In this area, the elongated pearlite lamellae were almost parallel to the outermost layer; the average spacing between those lamellae decreased, approximately

ACCEPTED MANUSCRIPT

100-150nm, which mainly contributed to increasing hardness. In the pearlite lamellae structures, the different contrast of the ferrite grains was observed. In other words, the orientation of the ferrite grains increased.

It was noticed that the area in the fine-grained layer, at the depth span of 1.5-20μm, did not exhibited any pearlite lamellae structures. The features of submicrometer ferrite subgrains appeared and cementite plates were fragmented, as was shown in Fig.4(c-e). At the depth span of 13.5-20μm, the cementite plates transformed themselves to zigzag-like curved tracks, even began to fracture, and the ferrite subgrains with an average size of 100-150nm, were formed (Fig.4e). At the depth of 7-13.5μm (Fig.4d), cementite plates structure could not be observed; cementite plates were fragmented completely, with part of cementite resolved. In a depth span of 1.5-7μm was an equiaxed ferrite subgrains region（Fig.4c）,where the average size of equiaxed ferrite subgrains was about 100-120nm, and the cementite was grain-like, approximately 50-80nm, segregated at ferrite grain boundaries.

In the outermost layer, the microstructure was severely refined, shown in Fig.4(b).The ferrite grains had the size less than 100nm, and the cementite particles featured uniform distribution in this region, and most cementite grains refined themselves, with the size of only 10-30nm, but some cementite grains coarsed themselves to the size of 100nm. In a word, after dry sliding wear, the microstructure of pearlitic wheel steel had undergone dramatic changes.

In the following section, during the sliding wear process, the microstructure evolution and formation mechanism of nanocrystalline grains within the range of 50μm from the outermost layer will be discussed in detail.

3.3 TEM Investigations of the Nanometer-sized Grains Evolution Process

Generally speaking, the sections at different depths possessed different microstructural changes, which meant that these sections owned different plastic deformation mechanisms. Previous SEM investigations indicated that based on microstructure morphologies, the hardening region from the outermost layer to the inner substrate could be divided into three regions: the nanocrystalline region, the submicrometer region and the deformed region. These three regions were similar to those of previous studies[35-39], which indicated the SMAT-affected zone could also be divided into these three regions.

3.3.1 The Deformed Region

Through TEM, the deformed regions at low strains bordering on those with strain-free substrate (20-50μm deep from the topmost surface) were observed from two different directions, as was showcased in Fig.5. In this section, three typical deformation-induced microstructure feature could be identified: dislocation lines (DLs), dislocation tangles (DTs) and dense dislocation walls (DDWs). Closer to the outermost layer, DLs were denser. However, the dislocation distribution was not uniform. As was showcased in Fig.5, higher dislocation density appeared in ferrite grains, especially from the observation of longitudinal-section. For DTs, their arrangement was random without any preferable sliding orientations. Nevertheless, DDWs were frequently identified inside some ferrite grains from the observation of cross-section, shown in Fig.5. In a word, in this region, pearlite underwent obvious plastic deformation and the majority of lamellar directions parallelled with the sliding surface. Lamellar spacing obviously shrank, between 250-300nm, and inside the ferrite lamellae a great amount of dislocations took form. At the same depth, inside the ferrite of

ACCEPTED MANUSCRIPT

the longitudinal section featured dislocations and tangles; however, from the observation of the cross section, inside large amounts of ferrite appeared dislocation walls, which broke up ferrite, and some cementite fracturerd(Fig.5. as was shown by white arrows).

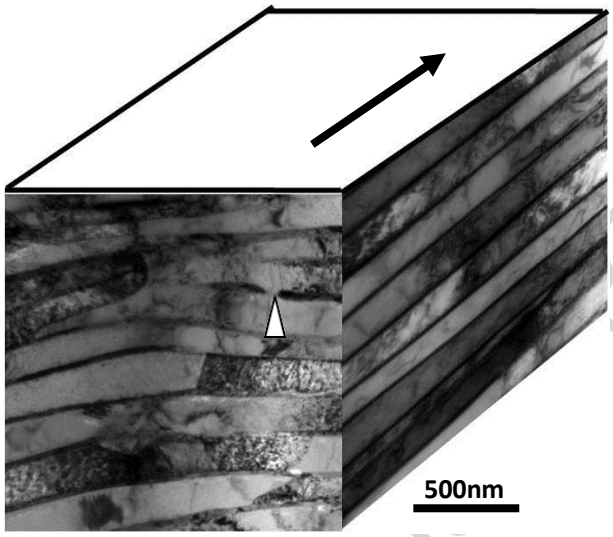

Fig.5 TEM Micrograph Showing the Deformed Region from Different Directions

3.3.2 The submicrometer region

With decreasing depths, deformation strains and strain rate increased. Within the submicrometer region, depth span of 1.5-20μm, original pearlite lamellar spacing further shrank, massive proportions of original ferrite grains were subdivided into submicro-sized grains, and cementite plates were fractured even resolved, as was shown in Fig.6(a).

In the cross-section, shown the BF image in Fig.6(b), the ferrite structure was very homogeneous, original lamellar structure could not be identified, primarily in approximately equiaxed shape with the average size in the range 100-200nm. Inside ferrite, considerable dislocations no longer existed, because with increasing strains, a large number of dislocations occurred at the ferrite-cementite interface. Concentric rings of spots, which proved the refined ferrite grains possessed high-angle misorientations, were observed from the SAED patterns (Fig.6c). Apart form ferrite diffraction rings, faint cementite diffraction rings could be observed, which signified that at this moment cementite had already become nanocrystalline grains with random orientation. From the DF images in this area, the size of cementite grains was extremely small, with the maximum size of 70nm. From paired observation between bright field images and dark field images, it could be found that fragmented yet undissolved cementite grains dispersed at the ferrite boundaries.

In the longitudinal-section(Fig.6d), the lamellar-shaped ferrite cell structures, with the thickness of about 100-200nm and the length of about 100-500nm respectively, were quite analogous to lamellar-type boundaries in heavily deformed metals[40 ,41] and Fe by tension experiments [42,43].
The lamellar ferrite cells were separated by evident subboundaries in the long axis. At smaller depth from the outermost layer, with increasing strain, the quantity of subboundaries increased accordingly, so that the lamellar ferrite cells were cut into more cells with smaller length/thickness ratios. These subboundaries were apparently sharper and thinner than the DDWs. It was commonly accepted that these subboundaries evolved from DDWs through the process where

ACCEPTED MANUSCRIPT

more dislocations accumulated and annihilated themselves and the misorientations across these subboundaries were much larger than those for DDWs[44].

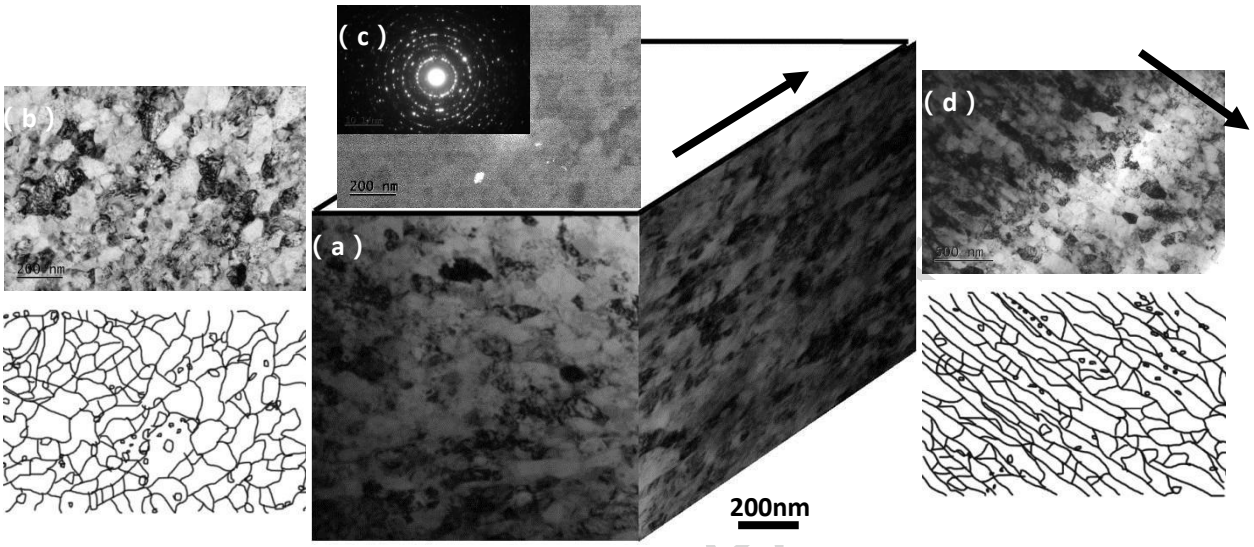

Fig.6 (a)TEM Micrograph Showing the Submicrometer Region from Different Directions at 5μm below the Sliding Wear Surface; (b)and(c) BF/DF Images with the Corresponding SADE Patterns of the Cross-section in the Submicrometer Region; (d) Typical Microstructures of the Longitudinal-section in the Submicrometer Region

3.3.3 The Nanocrystalline Region

In the outermost layer, the deformation strain and strain rate were drastically increased. Nanocrystalline grains were identified in the region from the outermost layer to 1.5μm deep. Typical microstructure in this region was shown in Fig.7 from the longitudinal-sectional and cross-sectional observations.

In the cross-section, a homogenous equiaxed nanocrystalline type was formed in the outermost surface region after dry sliding wear. As the BF image in Fig.7(a) and the DF image in Fig.11(b) showed, nanocrystalline grains, primarily in equiaxed shape (with sizes ranging from 10-30nm), were found at the topmost surface of 0.5μm thick and about 70nm at the depth ranging from 0.5-1.5μm from the outermost layer, without evident lamellae structure. The SAED pattern displayed ferrite polycrystalline rings and cementite spots, as was shown in Fig.7(b), which indicated that nano-sized ferrite grains with random orientations and cementite particles existed in this region.

Close to the outermost layer, equiaxed nanocrystallites with the size of about 10-30nm were spotted, and short rod-like shaped nanograins of 25-50nm short and 100-200nm long were present at the depth span of 0.5-1.5μm in longitudinal-section. It was notable that inside the inner of these short rod-like shaped nanograins, there existed even smaller equiaxed nanograins, as was shown in Fig.7(c). Evidently, these equiaxed nanograins were formed by breaking up the short rod-like shaped nanograins in that dislocation accumulation and subboundary development occurred, as in the case of submicrometer region. Then, with further straining, the misorientations between the bordering nanocrystallites progressively increased to high angles. As a result, equiaxed nanocrystallites possessed random orientations, as was presented by the SAED pattern.

The nanocrystalline grains in the outermost layer were closely observed by using HRTEM, as was elaborated in Fig.8. The nanocrystalline grains, which possessed different misorientations,

ACCEPTED MANUSCRIPT

were apparently identified, including high angles (nanocrystalline grain a and b) and low ones (nanocrystalline grain b and c, about 8°). The HRTEM imaging also confirmed that there existed cementite nano-level grains in the nanocrystalline region. On the left bottom of Fig.8, d grain, with 0.2nm interplanar spacing, featured the typical bcc structure, which corresponded to that of ferrite nanocrystalline grains (110); on the right top of Fig.8 was e grain, whose interplanar spacing was 0.41nm, shown from the magnified inset. The maximum interplanar spacing of ferrite bcc structure was 0.286nm (110), so an imaging pattern like this did not match a bcc structure. Since cementite orthorhombic structure had a larger interplanar spacing, e grain was cementite nanocrystalline grain (110).

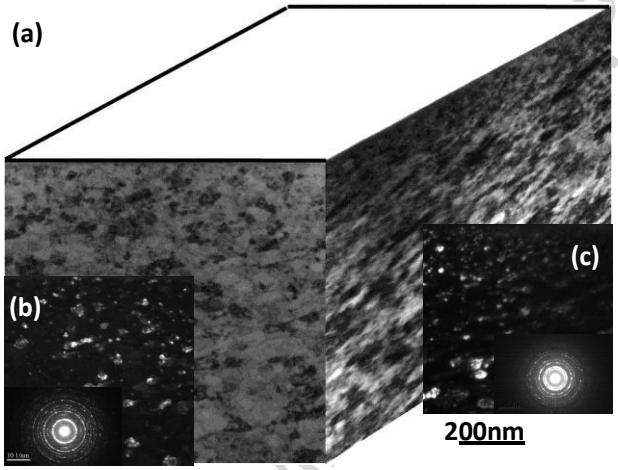

Fig.7 TEM Micrograph Showing the Nanocrystalline Region from Different Directions at the Topmost Surface; (b)and (c) Respectively Correspond to DF Images with the Corresponding SADE Patterns of the Cross-section and Longitudinal-section

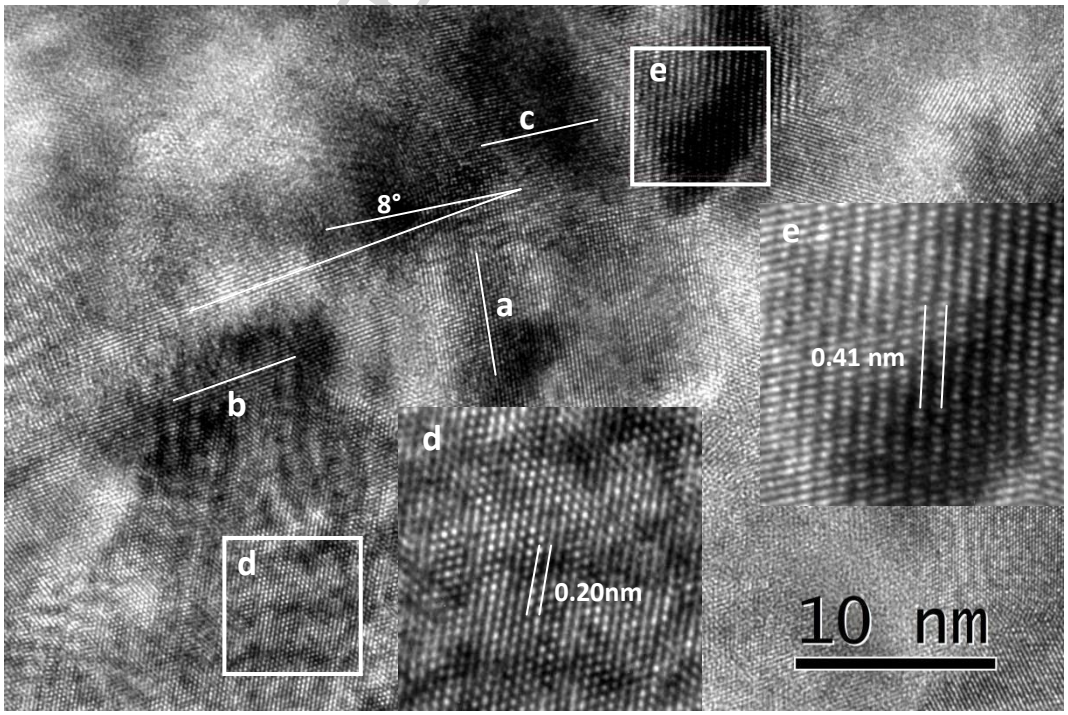

Fig.8 A HRTEM Image from the Outermost in the Nanocrystalline Region

ACCEPTED MANUSCRIPT

3.4 Mechanism of surface nanocrystallization of pearlitic wheel steels during the dry sliding wear process

Microstructural investigations revealed that nanocrystalline structures formed in the sliding wear surface of the pearlitic wheel steels after dry sliding wear. According to the microstructural observation of sliding wear at different depths (different deformation strains and strain rates) by SEM and TEM, what could be discovered was the formation of naocrystalline grains included the following processes:

1. Plastic deformation took place: pearlite lamellae were vertical to the direction of compressive stress, which caused their spacing to diminish, a small amount of cementite fractured and dissolved and considerable dislocations appeared inside ferrite;
2. Inside ferrite, dislocations tangled and formed dislocation walls, which broke up lamellar ferrite into many short-rod shaped and even aquiaxed small crystal cells, and at the same time, cementite commenced to dissolve considerably into particles;
3. Newly-formed ferrite low-angle sub-boundaries were transformed into HABs, whose grains were randomly oriented.
4. Under higher strain and strain rate, refined ferrite grains repeatedly underwent plastic deformation, the formation of dislocation cells and the transformation from LABs to HABs, until finally the size of ferrite grains reached the stable minimum value and the refinement of grains ceased.

The formation process of nanocrystalline grains could be schematically illustrated in Fig.9, in which each process would be fully discussed based on the experimental observations.

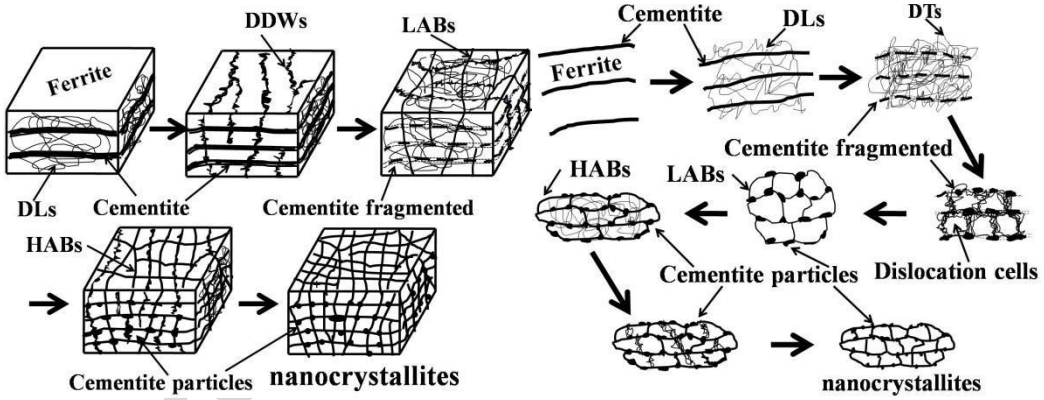

Fig.9 Schematic Illustration of the Nanocrystalline Formation Process of Pearlitic Steels by Dry Sliding Wear: (a) 3D View; (b) 2D View of the Cross-section

3.4.1 Plastic deformation

At the initial stage of dry sliding wear, pearlite at the outermost layer underwent plastic deformation—pearlite lamellae were vertical to the direction of compressive stress, which caused their spacing to diminish, and inside ferrite grains, large amounts of dislocations appeared.

Obviously, the pearlitic lamellar spacing decreased with increasing pressure, and the correlation between strengths and the lamellar spacing conformed to Hall-Petch relationship[45].As was shown in Fig.3 Hardness Distribution, it could be obviously observed that near the region of plastic

deformation, closer to the sliding wear surface, pearlite lamellar spacing was smaller and hardness

ACCEPTED MANUSCRIPT

was higher.

ACCEPTED MANUSCRIPT

ACCEPTED MANUSCRIPT

In the process of plastic deformation, although cementite had limited ductility, cementite plates and ferrite in pearlite deformed simultaneously; additionally, cementite plates even fractured into small particles featuring planar arrays, and a small amount of these particles even dissolved. Cementite deformation and reduction of cementite plates facilitated further cementite deformation, enlarged the interface area and enhanced the destabilization of cementite. Based on Gibbs-Thompson Effect, cementite dissolution would occur[46,47].

3.4.2 Formation of dislocation cells

For polycrystalline materials, for the purpose of accommodating plastic strains, multitudes of dislocation activities normally appeared, involving sliding, accumulation, interaction, tangling, and spatial rearrangement[48]. With increasing strain, in the pearlite that had already undergone plastic deformation, ferrite lamellar spacing continued to diminish, dislocation activities gave rise to the formation of DDWs and DTs in original ferrite grains of the outermost layer, and cementite plates also thinned continuously and were easy to fracture and dissolve, but they still arrayed in their original positions.

Progressive development of these dislocation configurations, such as DDWs andDTs, formed the individual dislocation cells that subdivided the original ferrite grains. Normally, the size of dislocation cells inside original ferrite grains reflected the spacing of DDWs. However, the relationship between dislocation cell dimensions (L) and the acting shear stress (τ) conformed to the function $L=10Gb/\tau$, in which G was the shear modulus and b was the Burgers vector[49]. Obviously, closer to the sliding wear surface, the larger the shear stress was; accordingly, the lattice dislocation density increased more and DDWs spacing and dislocation cell sizes inside ferrite were smaller. Meanwhile, at the same depth, shear stress on the longitudinal section was obviously larger than that on the cross section, so the size of dislocation cells on the cross section was smaller. Consequently, from the 3D perspective, during the process of dry sliding wear, ferrite lamellae were firstly cut into plate-shaped ones, parallel to the sliding direction, as was shown Fig. 9(a).

Nevertheless, with regard of cementite, the thinning of cementite plates resulted from deformation had its own limit, which consequently would weaken the tendency of cementite dissolution in accordance with the Gibbs-Thompson effect. Dislocation accumulation would enhance cementite dissolution because dislocation density increased and the contact area between cementite and dislocations enlarged correspondingly. That the bingding enthalpy between carbon atoms and dislocations in ferrite(~0.8eV[50-53]) exceeded the solution heat of cementite in ferrite(~0.5eV[54]) was the driving force of the cementite dissolution during deformation[55-60].

3.4.3 Transformation from LABs to HABs

At a certain strain level, for the sake of reducing the total system energy, in DDWs and DTs, dislocation annihilation and rearrangement occur, which would transform the regions around DDWs and DTs into subboundaries (with increasing misorientations compared with the original DDWs) separating individual cells, but the subboundaries were also supposed to be LABs. As a result, the formation of subboundaries would definitely lead to the density reduction of lattice dislocations, as was clearly displayed in Fig.6.

As strains further increased, the grains adjacent to each other featured totally random orientations, and the sub-boundary misorientation increased progressively until all the LABs were

ACCEPTED MANUSCRIPT

transformed into HABs. In general, either more dislocation accumulation and annihilation in grain boundaries or rotation of grains (or grain boundary sliding) under certain strains would foster the increment of misorientations between neighboring grains. Grain sizes would directly affect rotation of grains—the smaller the grains, the more easily the rotation would happen.[61].

While ferrite grain refinement began, cementite continued to dissolve. However, under certain strains, cementite dissolution apparently occurred; with increasing deformation strains, cementite dissolution reached saturation, because carbon atoms on dislocations at the interface became saturated. Therefore, with increasing strain, cementite would not ceaselessly dissolve until it totally disappeared; there still would be undissolved and fine cementite that remained the original position—in the vicinity of ferrite boundary. Therefore, in SADE, cementite diffraction spots/rings could constantly be observed. Because cementite were extremely small, the spots/rings were relatively faint, as was shown in Fig.6(c).

3.4.4 Formation of nanostructures in the outermost layer

During the dry sliding wear, the deformation at the outermost layer of the sliding wear took place under extremely high strain rates; with increasing depths from the surface, the strain rate dropped drastically. At high strain and strain rates, grains（refined subgrains and ferrite grains） transformed themselves into nanosized rod-like shaped grains along the direction of shear stress, and the deformation-induced dislocation density could be extremely high. Inside short rod-like shaped subgrains and grains, DDWs and DTs took form, and subsequently dislocation cells and subgrains with nanosized width appeared, which eventually transformed into equiaxed nanocrystalline grains with highly misoriented by grain rotation. This was because the probability of grain rotation and grain boundary sliding would be higher for nanocrystalline grains compared with the coarse ones. During the process of dry sliding wear, as long as higher strain and higher strain rate existed, the above-mentioned transformation would continuously occur. As long as dislocations took form, cementite would continuously dissolve, which would make the size of cementite particles gradually become smaller. Only when dislocation multiplication rate and the annihilation rate were in equilibrium, ferrite grain refinement ceased and cementite particles would no longer dissolve and diminish, so a stabilized size of ferrite grains and cementite particles was resulted. However, under extremely high strains, in addition to cementite dissolution, dislocations pinned by carbon atoms would bow out. This was because when the external force was exerted to equiaxed nanosized ferrite, the dislocations bowed out between the pinning points. If the force exerted on carbon atoms exceeded the energy of bingding between the carbon atoms and the dislocations, the carbon atoms would be removed from the dislocations and gather to grow up.

4. Conclusions

(1) Nanocrystalline grains, whose average size was approximately 35±5nm, were generated in the outermost layer of a double-phase pearlitic wheel steel after dry sliding wear. The thickness of the nanocrystalline layer approximated 1.5μm.

(2) The nanocrystallization during dry sliding wear could be divided into four steps: plastic deformation took place, ferrite plate spacing became smaller, inside the ferrite large amounts of dislocations formed, cementite plates became thinner and some of them fractured and dissolved; dislocation cells formed inside ferrite and DDWs transformed into subboundaries;

ACCEPTED MANUSCRIPT

subboundaries transformed into HAGs; under higher strains and higher strain rates, refined ferrite grains repeatedly underwent the above-mentioned three processes, until finally ferrite grains reached the stable minimum size and formed nanocrystalline grains.

(3) During the process of grain refinement, cementite fractured and dissolved. When the strain was relatively small, cementite were mainly affected by Gibbs-Thompson Effect and small amounts of carbon atoms dissolved into ferrite; with increasing strain, multitudes of dislocations formed, the dissolved carbon atoms inside ferrite reached saturation and the remaining large amounts of carbon atoms dissolved in the dislocations in the vicinity of boundary; when dislocation multiplication rate and annihilation rate balanced, cementite dissolution ceased and the undissolved cementite particles remained their original positions.

Acknowledgements

This research was supported by National Key Basic Research Program of China (No. 2015CB654802) and Key Research Program of China Railway (No.2013J008-C)

References

[1] Tang JSC, Koch CC. Scr Metall Mater 1990;24:1599.

[2] Morris DG. In: Mechanical behavior of nanostuctured materials. Clausthal, Germany: Trans. Tech. Publications Ltd; 1998. p. 70.

[3] Cahn RW. Nature 1990;348:389.

[4] Bohn R, Haubopld T, Birringer R, Gleiter H. Scr MetallMater 1991;25:811. [5]

Lu K, Lu J. Mater Sci Eng A 2004;38:375.

[6] Wang K, Tao NR, Liu G, Lu J, Lu K. Acta Mater 2006;54:5281.

[7] Wu X, Tao N, Hong Y, Liu G, Xu B, Lu J, et al. Acta Mater 2005;53:681. [8]

Zhu KY, Vassel A, Brisset F, Lu K, Lu J. Acta Mater 2004;52:4101.

[9] H.Q. Sun, Y.-N. Shi, M.-X. Zhang, K. Lu, Plastic strain-induced grain refinement in the nanometer scale in a Mg alloy, Acta Materialia 55(2007), 975-982.

[10] Langford G. Metallurgical Transactions A 1977;8A:861. [11]

K. Maurer and D. H. Warrington, Phil. Mag. 15, 321 (1967).

[12] Gil Sevillano, J. Mater. Sci. Eng. 20, 221 (1975).

[13] A. Inoue, T. Ogura, and T. Masumoto, Trans JIM. 17, 149 (1977).

[14] K. Maurer, D.H.Warrington, Phil. Mag.15(1967)321.

[15] J.Gil Sevillano, Mater. Sci. Eng. 21 (1975) 221.

[16] A. Inoue, T. Ogura, T. Masumoto, J. Jpn. Inst. Met. 37 (1973) 875. [17]

A. Inoue, T. Ogura, T. Masumoto, Bull. Jpn. Inst. Met. 13 (1974) 653. [18] A.

Inoue, T. Ogura, T. Masumoto, Metall. Trans. 8(1977) 1689.

[19] A. Inoue, T. Ogura, T. Masumoto, J.u. Imai, Tetsu to Hagane 61 (1975)149.

[20] Massalski TB. Binary alloy phase diagrams. 2nd ed. Ohio: American Society for Metals, 1990.

[21] T. Tarui, T. Takahashi, S. Ohashi, and R. Uemori, Iron Steelmaker. 21, 25 (1994).

[22] T. Tarui, T. Takahashi, H. Tashiro, and S. Nishida, in Processing and Applications of Metal Wires, ed. H. G. Paris and D. K. Kim, p. 87, TMS, Warrendale, PA (1996).

[23] H. G. Read, W. T. Reynolds, Jr., K. Hono, and T. Tarui, Scripta Meter. 37, 1221 (1997). [24] F.

ACCEPTED MANUSCRIPT

Danoix, X. Sauvage, D. Julien, and J. Copreaux, Mater. Sci. Eng. A250, 8 (1998).

[25] M. H. Hong, W. T. Reynolds, Jr., T. Tarui, and K. Hono, Metall. Mater. Trans. 30A, 717 (1999).

ACCEPTED MANUSCRIPT

ACCEPTED MANUSCRIPT

[26] Y. Yamada, Trans. ISIJ. 16, 417 (1976).

[27] V. N. Gridnev, V. V. Nemoshkalenko, Y. Y. Meshkov, V. G. Gavrilyuk, V. G. Prokopenko, and O. N. Razumov. Phys. Stat.Sol. A31, 201 (1975).

[28] W. J. Nam, C. M. Bae, S. J. Oh, and S. J. Kwon, Scripta Mater. 42, 457 (2000).

[29] J. Languillaume, G.Kapelski, and B.Baudelet,Acta Mater.45,1201(1997).

[30] H.G. Read, W.T. Reynolds, Jr., K. Hono, and T. Tarui, Scripta Meter. 37,1221(1997).

[31] M. H. Hong, W. T. Reynolds, Jr., T. Tarui, and K. Honon, Metall. Mater. Trans. 30A, 717 (1999).

[32] Pan Rui, Chen Chunhuan, Ren Ruiming. A Method of Preparing SEM Specimen Including White Etching Layer: China, CN 105242075 A[P].2016-01-13

[33] Chen Chunhuan, REN Ruiming, Preparation for cross-sectional TEM specimen treated by self surfacenanocrystallization. PTCA (PART:A PHYS.TEST), 2009,45(11):680-683

[34] Y. Zhou, J.F. Peng, Z.P. Luo, B.B. Cao, X.S. Jin, M.H. Zhu, Phase and microstructural evolution in white ctvhing layer of a pearlitic steel during rolling-sliding friction[J], wear,2016

[35] Lu K, Lu J. Mater Sci Eng A 2004;38:375

[36] Tao NR, Wang ZB, Tong WP, Sui ML, Lu J, Lu K. Acta Mater 2002;50;4603

[37] Wu X, Tao N, Hong Y, Xu B, Lu J, Lu K. Acta Mater 2002;50:2075

[38] Wu X, Tao N, Hong Y, Liu G, Xu B, Lu J, et al. Acta Mater 2005;53:681.

[39] Zhu KY, Vassel A, Brisset F, Lu K. Lu J. Acta Mater 2004;52:4101.

[40] Rybin VV. Big plastic deformations and fracture of metals. Metallurgia, 1986.

[41] Hughes DA, Hansen N. Acta Mater 2000;11:2985.

[42] Langford G, Cohen M. Trans ASM 1969;82:623.

[43] Jago RA, Hansen N. Acta Metall 1986;34:1711.

[44] N. R. Tao et al. Acta Materialia 50 (2002) 4603-4616.

[45] J.D. Embury and R.M.Fisher, Acta Metall.14,147

(1966).

[46]J. Languillaume, G. Kapelski, B. Baudelet, Acta Mater. 45 (1997) 1201.

[47] X. Sauvage, J. Copreaux, F. Danoix, D. Blavette, Phil. Mag. A 80 (2000) 781.

[48]N. R. Tao et al. Acta Materialia 50 (2002) 4603-4616.

[49] Kuhlmann-Wilsdorf D, Van der Merwe JH. Mater Sci Eng 1982;55:79.

[50]G.A. Beresnev, V.I. Sarrak, N. A. Shilov, Problems of Metal Science and Metal Physics (in Russian),1968,

ACCEPTED MANUSCRIPT

p.157.

[51] M.E. Blanter, A.I. Surin, M.S. Blanter, in: A.S. Golovin (Ed.), Interaction Between Dislocations and Impurity Atoms and Properties of Metals, Tula Polytecnical Institute, Tula, 1974, p. 154.

[52] V.G. Gavriljuk, N.P. Kushnareva, V.G. Prokopenko, Phys. Met. Metall. 42 (1976) 1288.

[53] A.W.Cochardt, G. Schoeck, H. Wiedersich, Acta Metall. 3 (1955) 533.

[54] D. Kalish, M. Kohen, Mater. Sci. Eng. 6 (1970) 156.

[55] V.N. Gridnev, V.G. Gavriljuk, I.Y. Dekhtyar, Y. Y. Meshkov, V.G. Prokopenko, P.S. Nizin, Phys. Stat. Sol. (a) 14 (1972) 689.

[56] V.N. Gridnev, V.G. Gavriljuk, V.V. Nemoshkalenko, Y.Y. Meshkov, V.G. Prokopenko, O.N. Razumov, Phys. Stat. Sol.(a) 31 (1975) 201.

[57] V.G. Gavriljuk, Phy. Met. Metall. 45 (2) (1978) 59.

[58] V.G. Gavriljuk, V.G. Prokopenko, O.N. Razumov, Phys. Stat. Sol.(a) 53 (1979) 147.

[59] V.G. Gavriljuk, D.S. Gertsricken, Y.A. Polushkin, V.M. Falchenko, Phys. Met. Metall. 51 (1981) 147. [60] V.N. Gridnev, V.G. Gavriljuk, Phys. Met. 4 (1982) 531.

[61] Von Swygenhoven H, Farkas D, Caro A. Phys Rev B 2000;62:831.

ACCEPTED MANUSCRIPT

ACCEPTED MANUSCRIPT

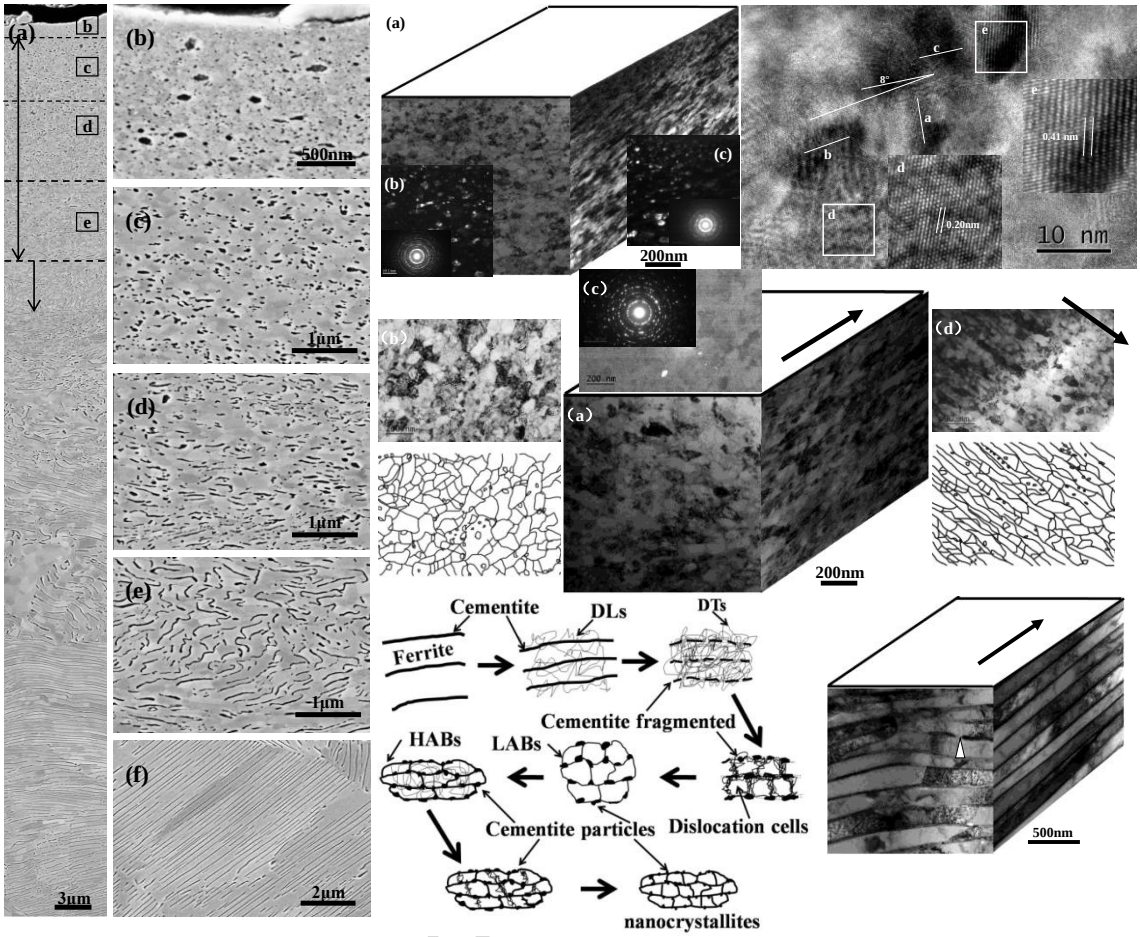

Graphical abstract

ACCEPTED

ACCEPTED MANUSCRIPT

Highlights

1. Nanocrystalline grains, whose average size was approximately 35±5nm, were generated in the outermost layer of a double-phase pearlitic wheel steel after dry sliding wear. The thickness of the nanocrystalline layer approximated 1.5μm.

2. Schematic illustration was employed to characterize the formation of nanocrystalline grains of pearlitic wheel steels during dry sliding wear.

3. The nanocrystallization during dry sliding wear could be divided into four steps: plastic deformation took place, ferrite plate spacing became smaller, inside the ferrite large amounts of dislocations formed, cementite plates became thinner and some of them fractured and dissolved; dislocation cells formed inside ferrite and DDWs transformed into subboundaries; subboundaries transformed into HAGs; under higher strains and higher strain rates, refined ferrite grains repeatedly underwent the above-mentioned three processes, until finally ferrite grains reached the stable minimum size and formed nanocrystalline grains.

4. During the process of grain refinement, cementite fractured and dissolved. When the strain was relatively small, cementite were mainly affected by Gibbs-Thompson Effect and small amounts of carbon atoms dissolved into ferrite; with increasing strain, multitudes of dislocations formed, the dissolved carbon atoms inside ferrite reached saturation and the remaining large amounts of carbon atoms dissolved in the dislocations in the vicinity of boundary; when dislocation multiplication rate and annihilation rate balanced, cementite dissolution ceased and the undissolved cementite particles remained their original positions.

ACCEPTED MANUSCRIPT